Draft version October 10, 2014
Preprint typeset using LaTeX style emulateapj v. 5/2/11

arXiv:1410.2269v1 [astro-ph.GA] 8 Oct 2014

NGC 7538 IRS 1: INTERACTION OF A POLARIZED DUST SPIRAL AND A MOLECULAR OUTFLOW

M. C. H. Wright[1], Charles L. H. Hull[1], Thushara Pillai[2], Jun-Hui Zhao[3], Göran Sandell[4]

Draft version October 10, 2014

ABSTRACT

We present dust polarization and CO molecular line images of NGC 7538 IRS 1. We combined data from the SMA, CARMA and JCMT telescopes to make images with $\sim 2.5''$ resolution at 230 and 345 GHz. The images show a remarkable spiral pattern in both the dust polarization and molecular outflow. These data dramatically illustrate the interplay between a high infall rate onto IRS 1 and a powerful outflow disrupting the dense, clumpy medium surrounding the star. The images of the dust polarization and the CO outflow presented here provide observational evidence for the exchange of energy and angular momentum between the infall and the outflow. The spiral dust pattern, which rotates through over 180° from IRS 1, may be a clumpy filament wound up by conservation of angular momentum in the infalling material. The redshifted CO emission ridge traces the dust spiral closely through the MM dust cores, several of which may contain protostars. We propose that the CO maps the boundary layer where the outflow is ablating gas from the dense gas in the spiral.

Subject headings: stars: formation — ISM: molecules — ISM: kinematics and dynamics — ISM: jets and outflows — ISM: H II regions — radio lines: ISM

1. INTRODUCTION

NGC 7538 IRS 1 is a young, heavily accreting hypercompact (HC) H II region located at a distance of 2.65 kpc (Moscadelli et al. 2009). IRS 1 drives a well collimated bipolar ionized jet north-south (N–S) in the central 0.025 pc ($2''$) region (Campbell 1984; Gaume et al. 1995; Sandell et al. 2009). With an IR luminosity of $10^5\,L_\odot$ (Willner 1976; Akabane & Kuno 2005), IRS 1 is also believed to be the energy source driving the CO ouflow, which extends NW–SE for 0.5 pc ($40''$) (e.g., Scoville et al. 1986; Kameya et al. 1989; Davis et al. 1998; Qiu et al. 2011). Single-dish data from the Five College Radio Astronomy Observatory (FCRAO), the Onsala Space Observatory (OSO), and the James Clerk Maxwell Telescope (JCMT), along with interferometric data from the Very Large Array (VLA), Berkeley-Illinois-Maryland Array (BIMA), Combined Array for Research in Millimeter-wave Astronomy (CARMA), and Submillimeter Array[5] (SMA) show that the molecular outflow extends N–S at distances of > 2 pc ($2.5'$) (Sandell et al. 2012). Precession has been suggested to explain why the inner ionized jet (0.025 pc) and the molecular outflow are misaligned (Kraus et al. 2006).

The spectral line profiles in ^{13}CO(2–1), CO(2–1), and HCN(1–0) observed toward IRS 1 show broad redshifted absorption, providing evidence for gas with an infall rate of $3-10\times10^{-3}\,M_\odot\,yr^{-1}$ (Zhu et al. 2013). Observational evidence for an accretion disk is controversial. A structure oriented NE–SW is observed in the mid-infrared (De Buizer & Minier 2005), as is a velocity gradient in the molecular lines (Brogan et al. 2008; Klaassen et al. 2009; Beuther et al. 2012; Zhu et al. 2013). A NW–SE velocity gradient of $\sim 0.02\,km\,s^{-1}\,AU^{-1}$ found in methanol masers (Minier et al. 1998, 2000) was modeled as a circumstellar disk (Pestalozzi et al. 2004). However, failing to find convincing evidence for an accretion disk from the sub-arcsec resolution observations with SMA and CARMA, Zhu et al. (2013) suggested that a rotating ionized outflow could entrain the adjacent molecular gas, and the impact of the ionized outflow on the circumstellar gas could produce highly excited molecular species in the regions NE and SW of IRS 1.

Recent dust polarization observations at 230 GHz (Hull et al. 2014) and 345 GHz (Frau et al. 2014) reveal a spiral distribution in both the dust emission and the magnetic field (B-field) inferred from dust polarization. Here we present dust polarization and CO molecular line images of NGC 7538 IRS 1. We combined data from the SMA, CARMA and JCMT telescopes to make images with $\sim 2.5''$ resolution at 230 and 345 GHz. We discuss the possible origin of the remarkable spiral pattern observed in the molecular outflow, the dust emission, and the B-field.

2. OBSERVATIONS AND DATA REDUCTION

2.1. *SMA Data*

The SMA CO(3–2) line image was made from the SMA archival data observed on three consecutive days (2005 Oct 05, Oct 06, and Oct 07) in a compact array configuration, and centered on IRS 1 at a position RA(J2000) = 23:13:45.36, Decl(J2000) = +61:28:10.6 in the NGC 7538 complex. The observing frequency was set at $\nu_{LO} = 341.5$ GHz in a circular polarization correlator mode with 24 adjacent spectral windows for each sideband; each of the two sidebands contains 128 spectral channels with widths of 0.812 MHz. The upper sideband

[1] Department of Astronomy, University of California, Berkeley, Berkeley, CA 94720, USA
[2] Max Planck Institut für Radioastronomie, Auf dem Hügel 69, 53121 Bonn
[3] Harvard-Smithsonian Center for Astrophysics, 60 Garden Street, Cambridge, MA 02138, USA
[4] SOFIA-USRA, NASA Ames Research Center, MS 232-12, Building N232, Rm. 146, P.O. Box 1, Moffett Field, CA 94035-0001, USA

[5] The Submillimeter Array is a joint project between the Smithsonian Astrophysical Observatory and the Academia Sinica Institute of Astronomy and Astrophysics and is funded by the Smithsonian Institution and the Academia Sinica.

(USB) contains the CO(3–2) line at $\nu_0 = 345.796$ GHz. The data reduction was processed in MIRIAD. The RR and LL visibility data were extracted prior to calibrations. Mars and/or 3C454.3 were used for bandpass calibration. The complex gains were calibrated using BL Lac and the flux-density scale was determined using Uranus. The baseline-based corrections were made using the point-source model determined from 3C111. The residual errors in the gain were further corrected by using the unresolved continuum source at IRS 1. The corrections for the residual errors were applied to the CO line data in which the continuum level was subtracted using the MIRIAD task UVLIN with a linear fitting.

The visibility channel data were binned to a velocity width of 1 km s^{-1} to make spectral line images with robust=2 weighting. The synthesized image was cleaned in MIRIAD using the default mode. The typical RMS noise is 0.35 Jy beam^{-1} per channel, with a synthesized beam FWHM of $2.40'' \times 2.05''$ (PA = 30.7°).

2.2. *CARMA Data*

Observations were made with CARMA between May 2011 and April 2013. Three different array configurations were used: C (26–370 m baselines, or telescope spacings), D (11–148 m), and E (8.5–66 m), which correspond to angular resolutions at 1.3 mm of approximately $1''$, $2''$, and $4''$, respectively. These data were combined to make images of the dust polarization and CO(2–1) emission with $\sim 2.5''$ resolution. The observations of NGC 7538 are part of the TADPOL survey. For details of these observations see Hull et al. (2014).

2.3. *JCMT Data*

CO(3–2) observations were made with JCMT in service mode under program ID M05AI07 on 2005 Apr 14, Apr 28, and May 20. These data were combined with the SMA data using the MIRIAD task IMMERGE to make well sampled images with angular resolution $\sim 2.5''$.

3. RESULTS

3.1. *Dust polarization*

Figure 1 summarizes the results of the CARMA polarization observations at 230 GHz (Hull et al. 2014). Similar results were obtained by Frau et al. (2014) at 345 GHz, confirming the remarkable spiral structure. The dust continuum emission is shown in color with the plane-of-the-sky (POS) component of the B-field (B_{pos}) overlaid as vectors. Throughout the field of view (FOV) there is a high polarization fraction ($\sim 6\%$) and remarkable alignment of the B-field vectors along a spiral structure centered on IRS 1. The only significant deviation of the B-field from the spiral pattern occurs near the dust clump MM5. The presence of many H_2O masers (Kameya et al. 1990) suggests that stars may already have formed in some of the dust clumps, with outflows that have disrupted the spiral B-field pattern. There is a marked decrease in the polarized fraction towards the center of IRS 1 ($\sim 1\%$), as observed towards most star forming regions, where depolarization creates a "hole" due to the star formation process itself.

Outside of IRS 1, we use clumps MM2 and MM3 (following Qiu et al. 2011), which have sufficient polarization for us to estimate the strength of the B-field using the Chandrasekhar-Fermi (CF) method (Chandrasekhar & Fermi 1953).

We can determine B_{pos} towards MM2/MM3 using $B_{pos} = f\sqrt{4\pi\rho}\,\delta V/\delta\phi$, where ρ is the gas density, δV is the velocity dispersion and $\delta\phi$ is the dispersion in the polarization angle and f is a factor of ~ 0.5 that corrects for any smoothing effect due to B-field averaging along the line of sight (LOS), provided the field is strong ($\delta\phi < 25°$) (Ostriker et al. 2001). Using the values from Table 1, we infer B_{pos} for MM2 and MM3 to be ~ 5.6 and 7.5 mG, respectively.[6]

A recently developed statistical approach to analyse the polarization angles allows us to estimate the contribution due to perturbations via the dispersion function, $1 - \langle cos[\Delta\phi(l)]\rangle$, where $\Delta\phi(l)$ is the difference in polarization angle between any pair of vectors separated by distance l (Houde et al. 2009). We apply this method to our data and refer the reader to Frau et al. (2014) for a discussion of the method and its specific application to the polarization data in NGC 7538. The 345 GHz data presented in Frau et al. are more sensitive to the dust emission and thus allow them to treat the spiral and the central source (IRS 1) separately. However, due to limited sensitivity in our 230 GHz data, we do not make this distinction. For the density and velocity dispersion listed in Table 1, and using our best fit value of the turbulent-to-large-scale magnetic field strength ratio of 0.59 ± 0.03, we derive a magnetic field strength of ~ 2.2 mG. This is consistent with the results from Frau et al.

3.2. *CO Outflow*

Figure 2 shows red- and blueshifted CO(3–2) outflows constructed from the image that combines SMA and JCMT data. We compared CARMA CO(2–1) and SMA CO(3–2) channel images at the same angular resolution. The CO(2–1) structure observed with CARMA shows the same clumpy distribution, in good agreement with the CO(3–2) structure observed with the SMA. The image combining SMA and JCMT data includes large scale structures that are not sampled by the interferometers, and reveals the connected spiral structure, which closely follows the B-field orientation and the dust emission.

4. DISCUSSION

4.1. *Interaction between the Magnetic field, Spiral Structure & Outflow*

The small-scale B-field direction is inconsistent with the NW–SE orientation of the large-scale B-fields from single-dish observations (Figure 36, Hull et al. 2014). On smaller scales the CO outflow, dust continuum and B-field morphology are consistent with a dominant spiral structure. This is suggestive of a direct interaction between the outflow, B-field and the accreting dense gas.

How do the energetics of the various physical processes compare? Qiu et al. (2011) have estimated the outflow energy to be 5×10^{46} erg. The magnetic energy corresponding to a B-field energy density $B^2/8\pi$ over a spher-

[6] Note that the CF method assumes that magnetic energy is in equipartition with turbulent energy. If the B-field alignment along the spiral is induced either by the outflow or infall, then the assumption of equipartition breaks down. Since the polarization angle due to turbulence is smoothed out by the spiral pattern, the derived field strengths reported in Table 1 are only upper limits.

ical volume of radius ~ 0.03 pc (this number corresponds to the radii of the MM2 and MM3 regions; see Table 1) is $\sim 1 - 2 \times 10^{45}$ erg. The spiral structure occupies 5-10% of the volume of the outflow, so that the energy density of the B field is comparable to that in the outflow. A similar conclusion was obtained by Frau et al. (2014) for the non-thermal energy. Thus, the ram pressure exerted by the massive outflow may be sufficient to drag and compress the magnetic field. However, the outflow may not be sufficiently powerful to penetrate and disrupt the dense accreting gas; we propose instead that the spiral structure may be deflecting the inner (lower-velocity) part of the outflow and moulding it into a spiral pattern along its boundary. Single-dish CO observations of IRS 1 covering a region a few arcmin in size (much larger than the region considered here) indicate that the outflow resumes its original N–S orientation further away from IRS 1 (Sandell et al. in prep.).

4.2. *Infall and Outflow*

At 1.3-mm wavelength, numerous molecular emission lines, including optically thin, high excitation energy levels which probe the innermost hot region (envelope/disk) of IRS1 (e.g. OCS, CH_3CN, CH_3OCH_3 and C_2H_5OH), show a strong emission peak at a radial velocity of -59.5 ± 1 km s^{-1} (Zhu et al. 2013). This value is close to the velocity component (-59.7 ± 0.3 km s^{-1}) observed in the mid-infrared by Knez et al. (2009). Figure 2 plots red- and blue-shifted CO 3-2 emission, more than 10 km s^{-1} from a systemic velocity of –59.5 km s^{-1} which we adopt in this paper.

The red- and blueshifted outflow traced in Figure 2 closely follows the B-field orientation and the dust emission. The redshifted CO emission shows a spiral structure starting from IRS 1, initially directed to the north, curving round at MM5 to the east, and continuing to change direction by more than 180°. The redshifted CO emission ridge traces the dust spiral closely through MM 1, 2, 5, 3, 6, 7, and perhaps as far as MM9. The blueshifted emission is initially directed to the SE within a few arcsec of IRS 1, then continues to the west, passing through a dust emission gap between MM2 and MM4 and extending toward the NW as observed in CO (1–0) on 100″ scales.

These results suggest substantial interaction between the outflow, and the spiral dust structure. Frau et al. (2014) detect 14 dust cores with masses 3.5 to 37 $M_\odot$, and a total mass 160 $M_\odot$, in which star formation may be enhanced by ram pressure from the outflow. They model the velocity pattern observed in the spiral as expansion at 9 km s^{-1}, and note that the outflow energy is comparable to the spiral arm kinetic energy. They suggest that the dust spiral is created from material swept up by the outflow.

Although the model they propose suggests that spiral dust feature and the magnetic field are tied to each other and are being pushed simultaneously by the outflow, it does not take infall into account, and does not explain why the massive MM cores and the filament remain aligned in a spiral pattern.

The infall and outflow have similar rates, $\sim 1-3\times10^{-3}$ $M_\odot$ yr^{-1} (Qiu et al. 2011; Zhu et al. 2013). The infall may have enough mass and momentum to deflect the outflow. An interesting alternative to Frau's expansion model is that the spiral structure is a clumpy infalling filament, or the remains of a filament in which IRS 1 has formed, and is now being ablated by the powerful outflow from IRS 1 (and possibly by other outflows in the region). The remarkable spiral structure, which rotates through over 180° from IRS 1, could be wound up by conservation of angular momentum in the infalling material. A rotation of 1 km s^{-1} would be sufficient to wind the spiral structure through 180 degrees in $\sim 4\times10^5$ yr. Although, currently, there is an energetically dominant outflow, the mass and angular momentum ultimately originate in the infall which created IRS1 and the compact MM sources. The total mass in the MM sources and the filament, estimated from dust emission is 160 $M_\odot$ (Frau et al. 2014). The current infall rate is $\sim 1 - 3\times10^{-3}$ $M_\odot$ yr^{-1} . An average infall rate $\sim 4\times10^{-4}$ $M_\odot$ yr^{-1} would accumulate 160 $M_\odot$ in $\sim 4 \times 10^5$ yr. This is also the right timescale to wind up the filament.

For comparison, Qiu et al. (2011) derive an outflow mass 50 $M_\odot$, energy 4.9×10^{46} ergs, dynamic time scale 2×10^4 yr, mass outflow rate 2.5×10^{-3} $M_\odot$ yr^{-1}, and momentum rate 2.3×10^{-2} $M_\odot$km s^{-1}yr^{-1}. In our model, the CO is mapping material ablated from the filament and reflects the radial velocity of the outflow, which is Frau et al's best fit. The observed CO (3-2) emission more than 10 km s^{-1} from the systemic velocity shown in Figure 2 maps material which has been swept up by the powerful outflow from IRS 1, and is consistent with the $H_{13}CO^+$ (4-3) and $C^{17}O$ (3-2) mapped by Frau et al. (2014) which also show the radial velocity of the outflow.

Submillimeter observations of NGC 7538 show filamentary dust ridges connecting IRS 1–3, NGC 7538 S, and IRS 9 (Sandell & Sievers 2004). Hershel observations show that NGC 7538 has a highly filamentary structure and multiple clumps with ongoing star formation (Fallscheer et al. 2013). These data suggest that the spiral structure may be filamentary material in the envelope around IRS 1.

Inverse P-Cygni profiles are seen towards IRS 1 in molecular lines with a wide range of excitation energy levels. Red-shifted absorption comes from dense gas in front of IRS 1 moving towards IRS 1. Blue-shifted emission comes from gas behind IRS 1 moving towards the observer (Qiu et al. 2011). Observations of HCO^+(1-0) by Corder (2008) & Sandell et al. (2009) suggest that the infall likely occurs within a region ~ 0.06 pc. Absorption features are detected in OCS(19-18) and CH_3CN(12-11) $k = 2$ - 5 in the velocity range between -56.5 to -53.0 km s^{-1}, corresponding to absorption features at -57.0 and -54.0 km s^{-1} in HCN(1-0), CO(2-1) and ^{13}CO(2-1) (Zhu et al. 2013). These absorptions are probably due to the redshifted absorption of the infalling gas, revealing the hot dense gas in the accretion flow. Absorption lines at higher excitation tracing warmer gas are more redshifted, perhaps tracing an accelerating infall closer to IRS1. The infall rate is estimated to be 1- 3×10^{-3} $M_\odot$ yr^{-1} (Qiu et al. 2011; Zhu et al. 2013).

Figure 3 shows the CO(3–2) spectra at the positions of the MM dust clumps. The spectra show multiple peaks corresponding to ambient and red- and blue-shifted gas at most locations, suggesting a turbulent, wide angle outflow interacting with clumpy, infalling gas. The blue

"jet" to the NW accelerates at increasing radius. Redshifted gas to the SE is more confined by higher densities. The CO(3–2) spectra are centered around +4 to +6 km s^{-1} with respect to the systemic velocity of ∼–59.5 km s^{-1}. The dip in the spectra around 4 to 6 km s^{-1} may be due to absorption of the hot outflow by colder infalling gas at a velocity of ∼4 to 6 km s^{-1} with respect to the systemic velocity. This is consistent with observations of the high-resolution absorption spectra of ^{13}CO(2–1) and CO(2–1) (Zhu et al. 2013). The infalling envelope is the ultimate source of the mass and angular momentum in the spiral.

Qiu et al. (2011) trace multiple outflows with an estimated total mass outflow rate $2.5{\times}10^{-3}$ $M_\odot$ yr^{-1} dominated by the outflow from IRS 1.

The molecular outflow mapped in CO traces material that has been swept up from the ambient medium by the powerful outflow from IRS 1. Figure 2 shows that the CO outflow follows the same spiral pattern traced by the polarized dust emission, which contains dense star forming cores. We propose that the red- and blueshifted CO shown in Figure 2 maps the boundary layer where the outflow is ablating gas from the dense gas in the spiral.

The images of dust polarization and CO outflow presented here provide observational evidence for the exchange of energy and angular momentum between the infall and outflow. This process is taking place throughout the infalling envelope as the outflow clears a way through the dense gas. In the paradigm model, a protostar creates an accretion disk that then transports angular momentum away from, and mass towards, the forming star. We have not seen the accretion disk, but we think it collimates the N–S ionized jet on subarcsec scales. A spiral structure extending into IRS1 could provide a ready explanation for the disparate position angles reported in dense gas close to IRS1 (Brogan et al. 2008; Klaassen et al. 2009; Beuther et al. 2012; Zhu et al. 2013; Minier et al. 1998, 2000).

But what happens further away from the protostar? Our observations suggest that the CO outflow is transporting angular momentum from a dense spiral structure traced in polarized dust emission. There could be significant angular momentum exchange in the infalling envelope, which would reduce the need to depend on a subarcsec accretion disk. A detailed mathematical model is beyond the scope of this paper, but the outflow could capture angular momentum from the infall in successive interactions. We may be seeing the process of an outflow transporting angular momentum from the infalling gas away from the forming star.

5. CONCLUSION

A high accretion rate continues to fuel star formation around IRS 1, where both an early type O star and a HC H II region have formed. The ionized outflow from IRS 1 is currently collimated in the N–S direction. The apparent rotation of the molecular outflow and polarized dust emission suggests significant interaction between the outflow and accreting material. The infall and outflow have similar rates, $\sim 1 - 3{\times}10^{-3}$ $M_\odot$ yr^{-1} . The spiral dust pattern, which rotates through over 180° from IRS 1, may be a clumpy filament wound up by conservation of angular momentum in the infalling material. The redshifted CO emission ridge traces the dust spiral closely through the MM dust cores, several of which may contain protostars. We propose that the CO maps the boundary layer where the outflow is ablating gas from the dense gas in the spiral.

The outflow transports angular momentum away from IRS 1 and may induce gravitational instability in the massive clumps in the spiral pattern forming protostars distributed around IRS 1.

C.L.H.H. acknowledges support from an NSF Graduate Fellowship and from a Ford Foundation Dissertation Fellowship. Support for CARMA construction was derived from the states of California, Illinois, and Maryland, the Gordon and Betty Moore Foundation, the Kenneth T. and Eileen L. Norris Foundation, the Associates of the California Institute of Technology, and the National Science Foundation. Ongoing CARMA development and operations are supported by the National Science Foundation under a cooperative agreement, and by the CARMA partner universities. The James Clerk Maxwell Telescope is operated by the Joint Astronomy Centre on behalf of the Science and Technology Facilities Council of the United Kingdom, the National Research Council of Canada, and (until 31 March 2013) the Netherlands Organisation for Scientific Research. We thank the anonymous referee for a careful reading and some good questions and suggestions which have improved this paper.

TABLE 1
Physical Parameters

Clumps	radius	δV	Mass	Density	$\delta\phi$	B_{pos}
	pc	km s^{-1}	$M_\odot$	10^6 cm^{-3}	rad.	mG
MM2	0.027	1.7	12.2	2.1	0.17	5.6
MM3	0.033	1.7	14.5	1.4	0.10	7.5

Notes: Mass and Density derived from CARMA 1.3 mm dust continuum assuming a dust temperature of 40 K over an effective area of radius $R = \sqrt{(A/\pi)}$ (Sandell & Sievers 2004; Qiu et al. 2011). We assume a dust opacity of 0.001 cm^2/g for dust grains with thin ice mantles and gas density n(H) = 10^6 cm^{-3} as in Ossenkopf & Henning (1994), and gas to dust ratio of 100. The velocity dispersion of 1.7 km s^{-1} corresponds to the maximum linewidth reported in Qiu et al. (2011) based on Gaussian fits to different spectral lines at 230 GHz.

REFERENCES

Akabane, K., & Kuno, N. 2005, A&A, 431, 183
Brogan, C. L., Hunter, T. R., Indebetouw, R., et al. 2008, Ap&SS, 313, 53
Beuther, H., Linz, H. & Henning, T. 2012, A&A, 543, 88
Campbell, B. 1984, ApJ, 282, L27
Chandrasekhar, S., & Fermi, E. 1953, ApJ, 118, 113
Corder, S. 2008, PhD thesis, Caltech
Davis, C. J., Moriarty-Schieven, G., Eislöffel, J., Hoare, M. G., & Ray, T. P. 1998, AJ, 115, 1118
De Buizer, J. M., & Minier, V. 2005, ApJ, 628, L151
Fallscheer, C., Reid, M. A., Di Francesco, J., & Martin, P. G. et al. 2013 ApJ773, 102
Frau, P., Girart, J. M., Zhang, Q., & Rao, R. 2014 http://adsabs.harvard.edu/abs/2014arXiv1405.6742F
Gaume, R. A., Goss, W. M., Dickel, H. R., Wilson, T. L., & Johnston, K. J. 1995, ApJ, 438, 776
Houde, M., Vaillancourt, J. E., Hildebrand, R. H., Chitsazzadeh, S., & Kirby, L. 2009, ApJ, 706, 1504
Hull, C. L. H., Plambeck, R. L., Kwon, W., et al. 2014, ApJS, 213, 13
Kameya, O., Hasegawa, T. I., Hirano, N., Takakubo, K., & Seki, M. 1989, ApJ, 339, 222
Kameya, O., Morita, K-I., Kawabe, R, & Ishiguro, M. 1990, ApJ, 355, 562
Klaassen, P. D., Wilson, C. D., Keto, E. R. & Zhang, Q. 2009, ApJ, 703, 1308
Knez, C., Lacy, J. H., Evans, N. J., II, van Dishoeck, E. F., & Richter, M. J. 2009, ApJ, 696, 471
Kraus, S., Balega, Y., Elitzur, M., et al. 2006, A&A, 445, 521
Minier, V., Booth, R. S., & Conway, J. E. 1998, A&A, 336, L5
Minier, V., Booth, R. S., & Conway, J. E. 2000, A&A, 362, 1093
Moscadelli, L., Reid, M. J., Menten, K. M., et al. 2009, ApJ, 693, 406
Ossenkopf, V., & Henning, T. 1994, A&A, 291, 943
Ostriker, E. C., Stone, J. M., & Gammie, C. F. 2001, ApJ, 546, 980
Pestalozzi, M. R., Elitzur, M., Conway, J. E., & Booth, R. 2004, ApJ, 603, L113
Qiu, K., Zhang, Q & Menten, K. M. 2011, ApJ, 728, 6
Sandell, G. & Sievers, A. 2004, ApJ, 600, 269
Sandell, G., Goss, W. M., Wright, M. & Corder, S. 2009, ApJ, 699, L31
Sandell, G., Wright, M., Zhu, L., et al. 2012, in ALMA/NAASC 2012 Workshop: Outflows, Winds and Jets (https://science.nrao.edu/facilities/alma/naasc-workshops/jets2012)
Scoville, N. Z., Sargent, A. I., Sanders, D. B., et al. 1986, ApJ, 303, 416
Willner, S. 1976, ApJ, 206, 728
Zhu, L., Zhao, J.-H., Wright, M. C. H., et al. 2013, ApJ, 779, 51

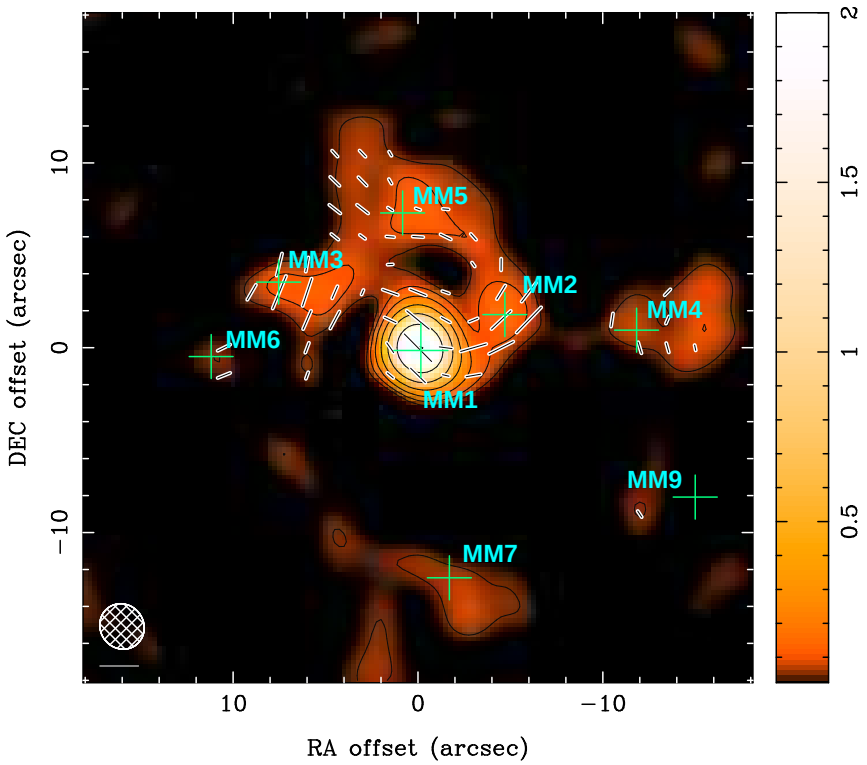

FIG. 1.— CARMA 1.3 mm B-field vectors overlaid on 1.3 mm dust continuum (colorscale and contours). Contours at 2,4,8,16,32,64,128 × 25 mJy beam^{-1}. The peak is 3.23 Jy beam^{-1}. The RMS noise in the dust continuum image is 19.3 mJy beam^{-1}. The color wedge on the right shows the color scale with a logarithmic range from 0.025 to 2 Jy beam^{-1}. The positions are offsets from IRS 1 at R.A. (J2000) = $23^{h}13^{m}45.^{s}37$, Dec. (J2000) = $61°28'10.''43$. The crosses mark the positions of SMA dust sources. The vectors of polarized intensity have been rotated by 90° to show the POS B-field orientation. The synthesized beam FWHM is drawn in the bottom left corner. The scale bar below the beam is drawn the length of the longest vector of polarized intensity, 11.6 mJy beam^{-1}. The RMS noise in the polarized intensity image is 0.7 mJy beam^{-1}.

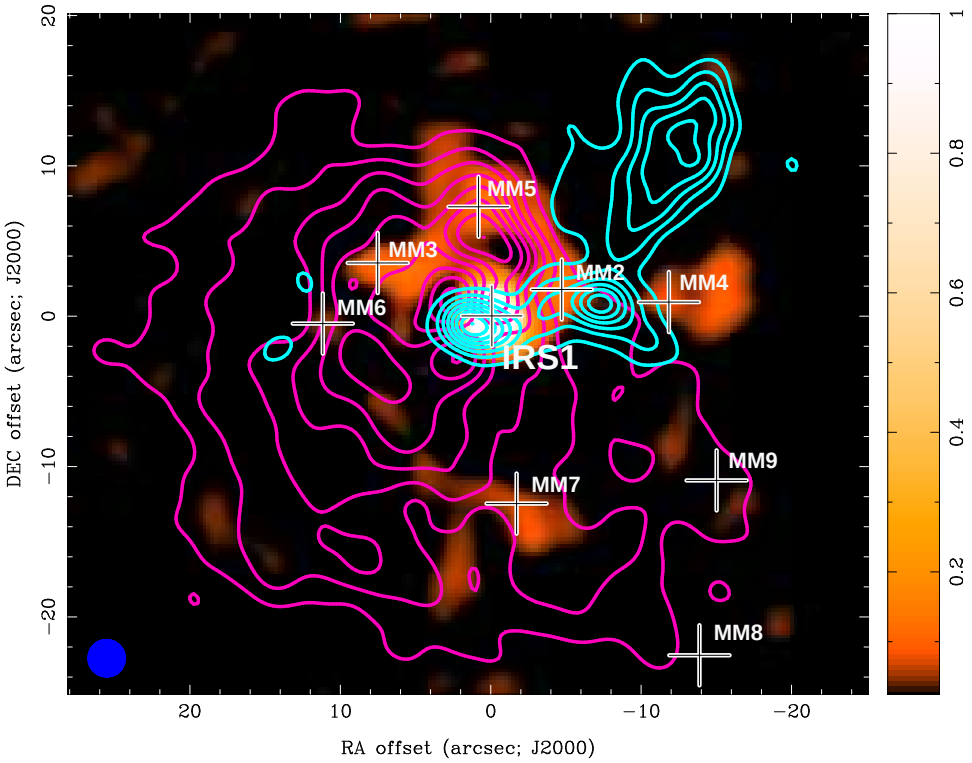

FIG. 2.— Red- and blueshifted CO(3–2) emission overlaid on the dust polarization color image at 230 GHz. The dust continuum (color scale) peak is 3.2 Jy beam^{-1}. The color wedge on the right shows the color scale with a logarithmic range from 0.025 to 1 Jy beam^{-1}. Magenta contours are in steps of 2.4 Jy beam^{-1} from 2.4 to 16.8 Jy beam^{-1} in velocity range 10 to 16 km s^{-1} from the systemic velocity –59.5 km s^{-1}. Blue contours are in steps of 1.025 Jy beam^{-1} from 1.025 to 8.203 Jy beam^{-1} in velocity range –10 to –16 km s^{-1} from the systemic velocity –59.5 km s^{-1}. The positions are offsets from IRS 1 at R.A. (J2000) = $23^{h}13^{m}45.^{s}37$, Dec. (J2000) = $61°28'10.''43$. The crosses mark the positions of SMA dust sources. The synthesized beam FWHM is drawn in the bottom left corner.

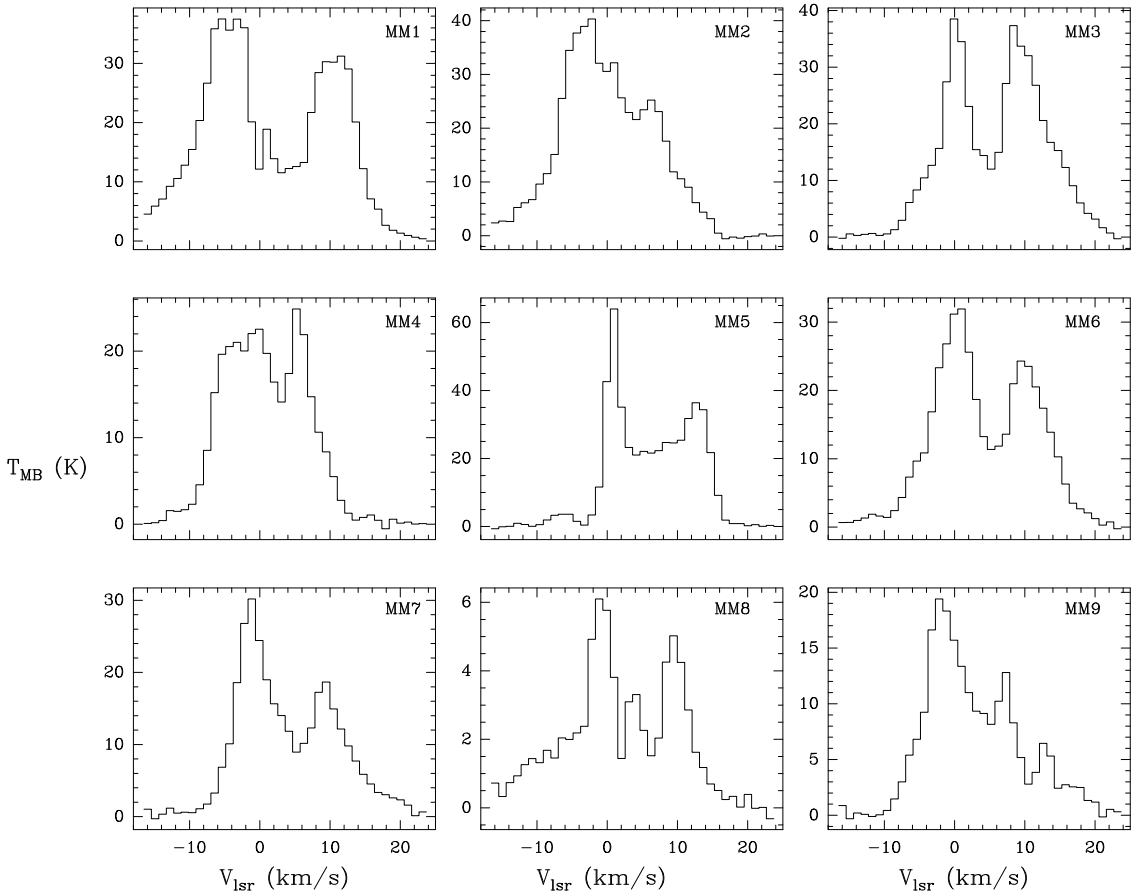

FIG. 3.— CO(3–2) emission from –16 to +23 km s^{-1} with respect to the systemic velocity –59.5 km s^{-1}. The CO(3–2) spectra at the positions of the MM sources marked in Figure 2. Offset positions are with respect to IRS 1 at R.A. (J2000) = $23^{\rm h}13^{\rm m}45.^{\rm s}37$, Dec. (J2000) = $61^\circ 28' 10.''43$.